Sfrp2 is a multifunctional regulator of rodent coat patterns

Matthew R. Johnson[1†], Sha Li[1†], Christian F. Guerrero-Juarez[2,3,4,5,6], Pearson Miller[7], Benjamin J. Brack[1], Sarah A. Mereby[1], Charles Feigin[1,8], Jenna Gaska[1], Alexander Ploss[1], Qing Nie[3,4,5,6], Jaime A. Rivera-Perez[8], Stanislav Y. Shvartsman[1,7], and Ricardo Mallarino[1*]

[1]Department of Molecular Biology, Princeton University; Princeton, New Jersey, 08540, USA.
[2]Carle Illinois College of Medicine, University of Illinois at Urbana-Champaign; Urbana, IL 61801 USA.
[3]Department of Developmental and Cell Biology, University of California; Irvine, Irvine, CA 92697, USA.
[4]Department of Mathematics, University of California, Irvine; Irvine, CA, 92697, USA
[5]Center for Complex Biological Systems, University of California, Irvine; Irvine, CA 92697, USA
[6]NSF-Simons Center for Multiscale Cell Fate Research, University of California; Irvine, Irvine, CA, 92697, USA
[7]Center for Computational Biology, Developmental Dynamics, Flatiron Institute, Simons Foundation; New York, New York, 10010, USA.
[8]Present address: School of BioSciences, The University of Melbourne, Parkville Victoria 3010, Australia
[9] Frederick National Laboratory for Cancer Research; Frederick, MA 21701, USA

† These authors contributed equally to this work

*Corresponding author. Email: rmallarino@princeton.edu

Abstract:
Animal pigment patterns are excellent models to elucidate mechanisms of biological organization. Although theoretical simulations, such as Turing reaction-diffusion systems, recapitulate many animal patterns, they are insufficient to account for those showing a high degree of spatial organization and reproducibility. Here, we study the coat of the African striped mouse (*Rhabdomys pumilio*) to uncover how periodic stripes form. By combining transcriptomics, mathematical modeling, and mouse transgenics, we show that *Sfrp2* regulates the distribution of hair follicles and establishes an embryonic prepattern that foreshadows pigment stripes. Moreover, using *in vivo* gene editing, we find that *Sfrp2* knockout produces changes in coat pattern. Strikingly, mutants also exhibit pigmentation differences, revealing an additional function of *Sfrp2* in regulating hair color. Thus, a single factor controls coat pattern formation by acting both as an orienting signaling mechanism and a modulator of pigmentation.

Introduction

The skin of many vertebrate species displays characteristic periodic pigment patterns, such as spots and stripes, which play key roles in mediating intra- and inter-specific communication (*1–3*). Theoretical simulations involving Turing reaction-diffusion systems, in which activators and inhibitors interact to establish organized spatial patterns, can closely recapitulate a wide variety of periodic color patterns seen in nature (*4–6*). Notably, however, Turing-generated patterns are variable and sensitive to stochastic perturbations (*7*). That is, Turing mechanisms are insufficient, by themselves, to explain the formation of periodic color patterns seen in many species, which are characterized by a high degree of spatial organization and reproducibility across individuals (*8–12*). Therefore, a long-standing challenge has been to uncover the molecular, cellular, and developmental events by which periodic color patterns are specified and organized.

The African striped mouse (*Rhabdomys pumilio*), a rodent that exhibits a naturally evolved coat pattern of dark and light parallel stripes (**Fig. 1A, B**), is a useful model in which to explore molecular mechanisms underlying periodic color patterns because this mouse can be maintained and reared in the lab, allowing for controlled experiments and development of molecular tools (*13*). Here, we use a variety of multidisciplinary approaches to uncover the developmental mechanisms controlling coat pattern formation in striped mice.

Striped mice display regional variation in embryonic placode formation

Striped mice exhibit differences in hair length between striped skin regions that are apparent at early postnatal stages (**Fig. 1B**) (*10*). We hypothesized that these differences may reflect stripe-specific alterations in the developmental timing of hair follicle placodes (hereafter referred to as placodes). In laboratory mice (*Mus musculus*), placodes are visible at embryonic day 15.5 (E15.5) and are evenly distributed throughout the dorsal skin (**Fig. 1C**) (*14, 15*). Remarkably, this stereotyped spatial pattern differs considerably in striped mice. At the equivalent embryonic stage (*i.e.*, the emergence of visible placodes, ~E16.5 in striped mice), whole mount *in situ* hybridizations for early markers of placode formation (e.g., *Dkk4, Ctnnb1, Wnt10b, Wif1, Eda,* and *Dkk1*) (*16*) revealed that striped mouse dorsal placodes develop in a stripe-like, spatially restricted manner, whereby they are present in some regions along the dorsal skin but absent in others (**Fig. 1C and fig. S1**). Approximately two days later, at E18.5, placodes eventually become visible in regions previously devoid of them, as evidenced by thickening of the epidermis and the appearance of molecular markers (**fig. S2**). Notably, stripe-like dorsal areas where placodes fail to form initially correspond to regions that will constitute the eventual dark pigment stripes, explaining why hair from dark stripes is shorter at birth and suggesting that spatially restricted patterns of embryonic placode formation foreshadow pigmentation stripes (**Fig. 1D**) (*10*).

Transcriptomics and mathematical modeling identify a potential regulator of placode patterning

To identify regulators of the striped mouse placode developmental pattern, we performed an unbiased bulk-level RNA-sequencing (RNA-seq) screen for genes differentially expressed between placode rich and placode barren skin regions in E16.5 embryos. We used the boundaries between these regions as a proxy to mark and isolate four distinct dorsal skin regions: R1 (the dorsalmost, placode barren region), R2 (the dorsalmost, placode rich region), R3 (the ventralmost, placode barren region), and R4 (the ventralmost, placode rich region) (**Fig. 2A**). Next, we performed a series of pairwise comparisons (R1 vs. R2; R1 vs. R4; R2 vs. R3; and R3 vs. R4) to

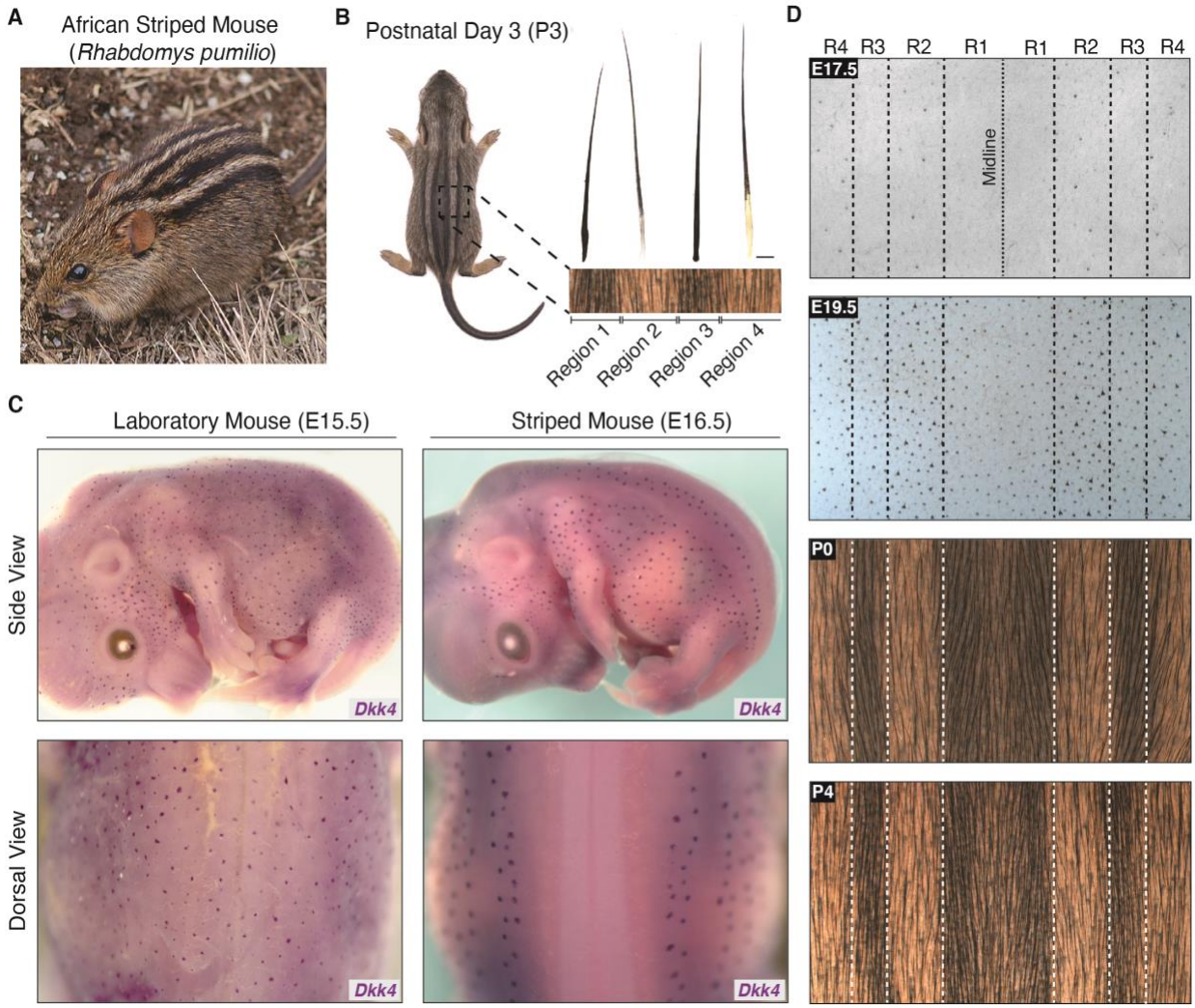

Fig. 1. Development of hair placodes and pigment patterns in the African striped mouse. (A) An adult striped mouse in the field. (B) Postnatal Day 3 (P3) striped mouse pup displaying the characteristic striped pattern and corresponding differences in hair length across dorsal regions. (C) Side and dorsal views of Embryonic Day 15.5 (E15.5) laboratory mouse and E16.5 striped mouse embryos displaying spatial patterns of hair placode formation, as visualized by whole-mount *in situ* hybridization for *Dkk4*. (D) Light-microscopy images of striped mouse flat mount skins from developmental and postnatal stages (E16.5 to P4) showing how patterns of hair placode development foreshadow pigmentation stripes. Photo credit in (A): Trevor Hardaker

identify differentially expressed genes between placode barren (R1, R3) and placode rich (R2, R4) regions. Although each pairwise comparison yielded several differentially expressed genes (**Fig. 2B, data S1**), only one gene, the Wnt modulator *Sfrp2*, was differentially expressed in all four comparisons. As Wnt signals are required for the initiation of hair follicle development (*16*), *Sfrp2* constituted an attractive candidate for patterning striped mouse placodes. Surprisingly, however, *Sfrp2* was neither up nor downregulated in placode barren (R1, R3) or placode rich regions (R2, R4). Rather, this gene was always upregulated in the dorsalmost region among the two being compared (*i.e.*, R1>R2, R1>R4, R2>R3, and R3>R4).

The dorsoventral expression pattern of a potential regulator of placode patterning was, *a priori*, unexpected. However, previous theoretical work has pointed to upstream morphogen gradients as a means for establishing stripe-like patterns (*17*). In mammals, placode spacing is regulated by a

self-organizing reaction-diffusion system in which activators and inhibitors interact to establish an organized spatial pattern (*18*). While the classic picture of stripe formation via a Turing instability features the emergence of patterns in response to global, spatially uniform perturbations, recent theoretical work has increasingly emphasized the capacity of spatial gradients to trigger the emergence of stripes (*19*). We therefore turned to mathematical modelling to verify that a dorsoventral gradient could be an effective mechanism for establishing stripes in a standard reaction-diffusion model. To demonstrate this point, we constructed a simple 1D model (**Fig. 2C)**, featuring an activator-inhibitor pair with the potential to generate pattern formation coupled to an upstream modulator, which catalyzes the degradation of the modulator. Such a model admits a

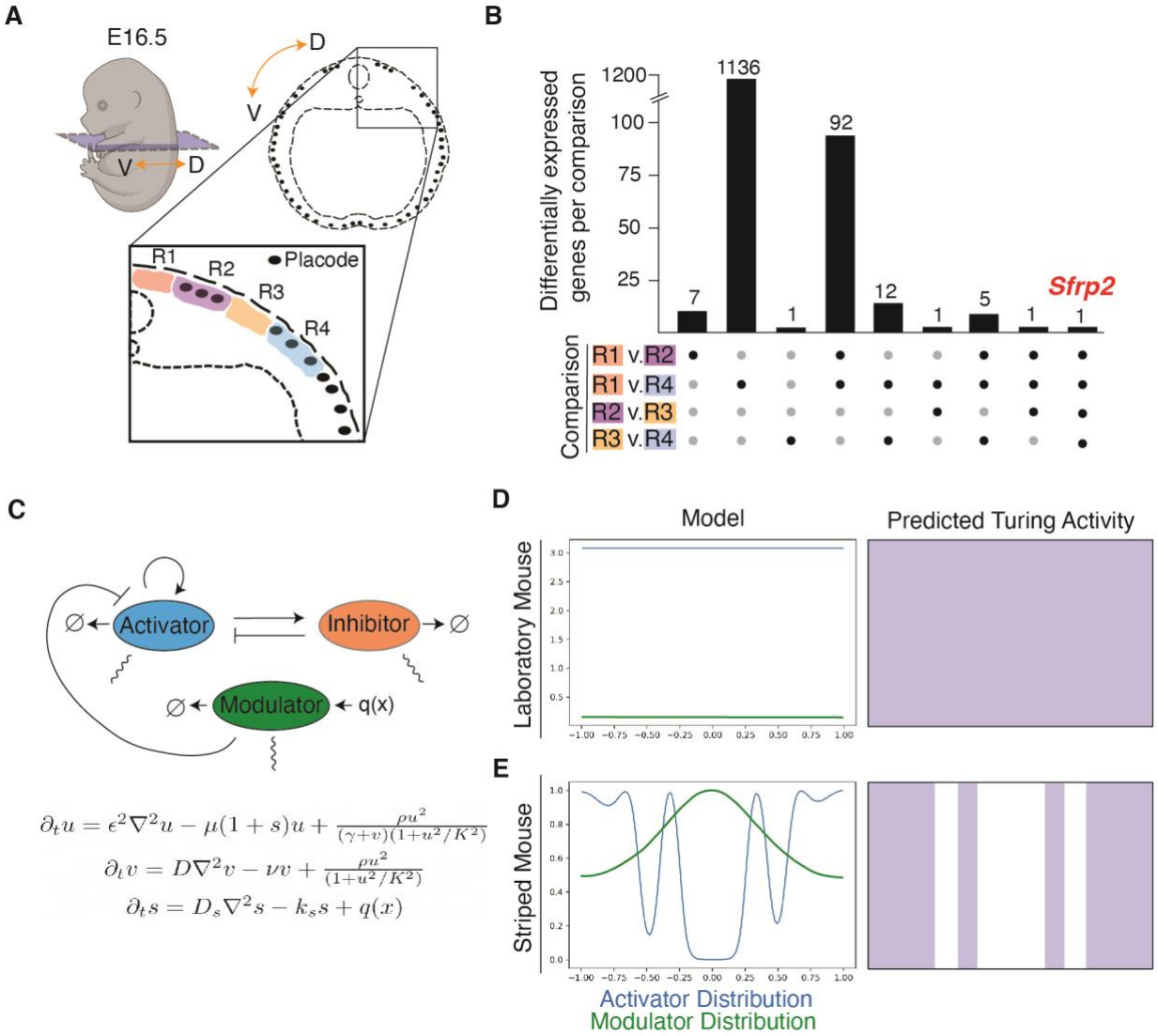

Fig. 2. Transcriptomics and mathematical modeling of placode development. (A) Schematic of an E16.5 striped mouse embryo displaying regions (R1-R4) dissected for bulk-level RNA-seq analysis. (B) UpSet plot summarizing differentially expressed genes (DEGs) (padj < 0.05) between R1-R4. Each row of dots represents a single pairwise comparison. Black dots indicate there were DEGs between a given comparison (number of DEGs plotted as columns) whereas grey dots indicate there were not. (C-E) Mathematical simulations of hair placode spacing in laboratory mouse and in striped mouse. (C) Equations used to model how a theoretical modulator (green) could guide the activity of an activator-inhibitor reaction-diffusion system. (D) Simulations of a uniform modulator expression pattern (green line) produces a uniform pattern of activity, consistent with what is seen in laboratory mice *in vivo* (Fig. 1C). (E) Simulations in which a dorsoventral gradient of a modulator (green line) applied to the same system in (D), leads to a stripe-like pattern of activity, recapitulating what is seen in striped mice *in vivo* (Fig 1C).

regime which is stable against pattern formation in the presence of uniform modulator expression (**Fig. 2D**) but becomes destabilized when the modulator is expressed as a dorsoventral gradient **(Fig. 2E**). This model, as well as alternative ones in which the behavior of the modulator varies (**fig. S3**), simulate patterns of Turing activity that closely resemble the placode patterns observed in laboratory mice and striped mice, respectively (*i.e.*, uniform Turing activity/placode in the lab mouse and striped regions of Turing activity/placodes in the striped mouse). Taken together, our modelling suggests that a dorsoventral gradient of *Sfrp2* could, in theory, contribute to stripe formation.

Importantly, while our computational analysis strongly implies that a dorsoventral orienting gradient can control the establishment of striped patterns, in nature there are likely multiple reinforcing, partially redundant mechanisms to assure phenotypic robustness. Thus, while *Sfrp2* emerged as a top candidate in our analysis, this gene is almost certainly part of a gene network acting in concert to establish such an orienting gradient. Indeed, our RNA-seq analysis identified other Wnt regulators expressed in a similar pattern, albeit at lower levels than *Sfrp2* and without statistically significant expression differences across all skin regions (**fig. S4**).

Taken together, our transcriptomic experiments coupled to our mathematical simulation data suggest that *Sfrp2*, a gene expressed in a dorsoventral gradient at a stage coinciding with the emergence of embryonic placodes, may constitute a key component of a dorsoventral orienting gradient regulating placode formation patterns in striped mice.

Sfrp2 expression correlates negatively with Wnt signaling

Sfrp2 is a known soluble regulator of Wnt signaling, having dual roles as both an activator and repressor, depending on cellular microenvironment (*20–23*). To uncover the relationship between *Sfrp2* and Wnt signaling in striped mouse skin, we dissociated dorsal skin from regions R1, R2, and R3 of E16.5 embryos, as before, and performed single-cell 3' - RNA-sequencing (scRNA-seq, 10X Genomics). We combined an equal number of cells from R1-R3 to generate a single pool representative of striped mouse E16.5 dorsal skin and identified fourteen distinct cell types based on expression of known molecular markers (**Fig. 3A, table S1**) (*24–26*). *Sfrp2* was specifically expressed in a subset of dermal fibroblasts, as judged by co-localization with canonical fibroblast markers (**Fig. 3B, table S1**). Next, we clustered cells based on *Sfrp2* expression to define a population of *Sfrp2*-high (i.e., > 2UMIs) and *Sfrp2*-low (i.e., < 2 UMIs) fibroblasts (**Fig. 3C**). Differential gene expression analysis between *Sfrp2*-high and *Sfrp2*-low cells yielded numerous genes (P_{adj} <0.05), 482 of which were upregulated and 272 that were downregulated in *Sfrp2*-high compared to *Sfrp2*-low cells (**data S2**). Among the genes upregulated in *Sfrp2*-low fibroblasts, Gene Ontology analysis identified regulation of Wnt signaling as the most significantly enriched pathway (**Fig. 3D**). Indeed, expression of numerous Wnt-related genes, including key activators of the pathway (i.e., *Lef1* and *Ctnnb1*), were higher in *Sfrp2*-low (**Fig. 3E, data S2**) compared to *Sfrp2*-high cells, demonstrating that *Sfrp2* and Wnt activation are negatively correlated in striped mice dermal fibroblasts.

To confirm and extend our previous observation, we examined spatial patterns of *Sfrp2* expression and Wnt signaling markers. RNA *in situ* hybridizations in cross sections from E16.5 striped mice embryos, coupled to immunohistochemistry (IHC) for an epidermal marker (KRT14), indicated that expression of *Sfrp2* was strong in mesenchymal cells directly above the neural tube and decreased laterally, a result consistent with our bulk-level RNA-seq analysis (**Fig. 3F**). At this same stage, immunofluorescence (IF) for LEF1 and CTNNB1 showed that these markers were

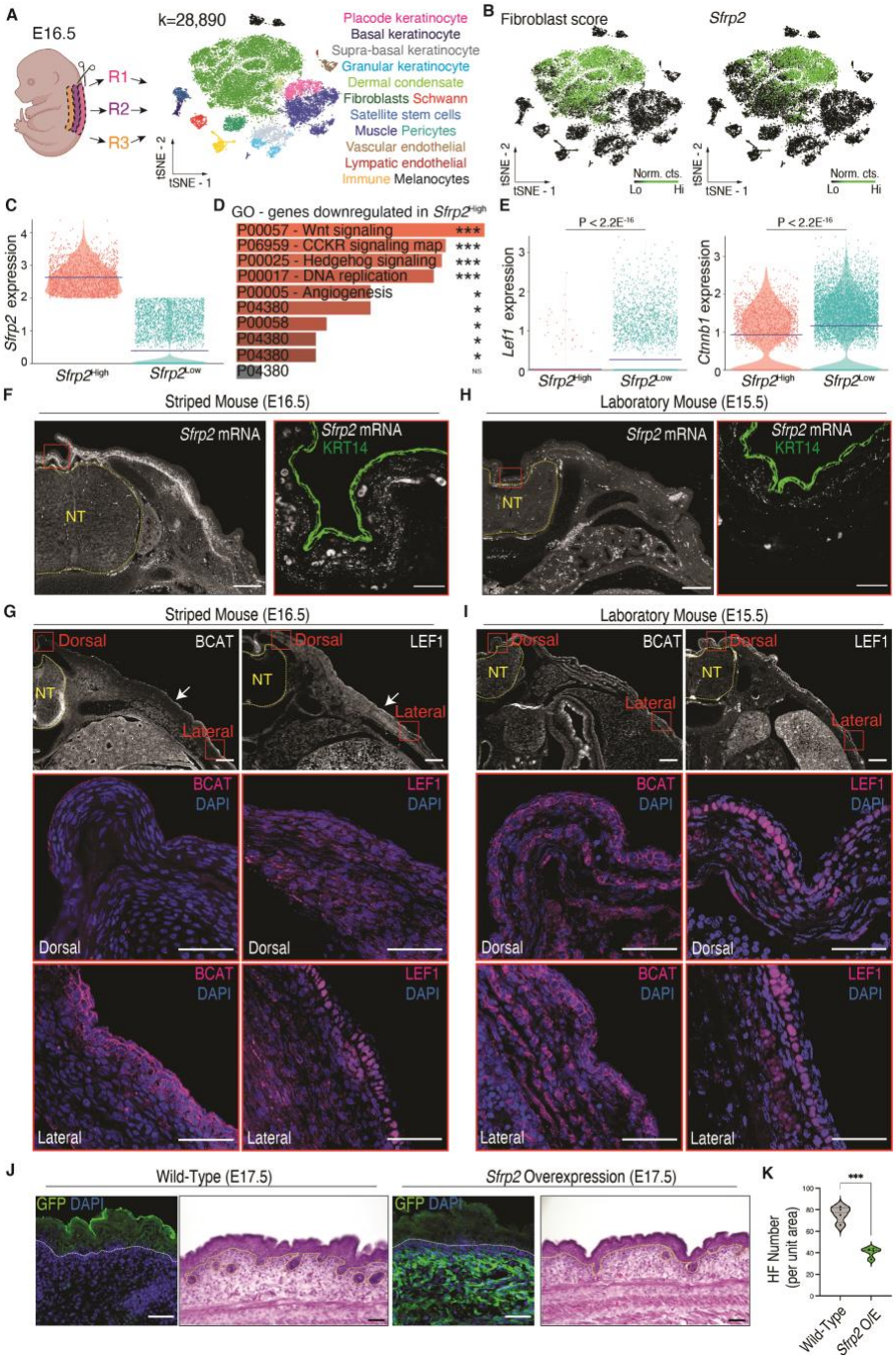

Fig. 3. Relationship between *Sfrp2* and Wnt signaling in embryonic skin. (A) Schematic of skin regions (R1-R3) dissected for scRNA-seq (left) and cell-type clustering (right). (B) Dermal fibroblasts (green, left) cluster with *Sfrp2* expressing cells (green, right). (C) Fibroblasts sorted by high (> 2 UMI) and low (< 2 UMI) *Sfrp2* expression. (D) Ontology analysis of genes downregulated in *Sfrp2*^{High} cells, show Wnt signaling as the main enriched pathway (Enrichr, Padj < 0.05). (E) *Lef1* and *Ctnnb1* show upregulation in *Sfrp2*^{low} cells (non-parametric Wilcoxon Rank Sum test). (F-H) *In situ* hybridization for *Sfrp2* coupled with immunofluorescence (IF) for KRT14 in stage-matched striped mouse (F) and laboratory mouse (H) embryos. (G-I) IF for CTNNB1 and LEF1 in stage-matched striped mouse (G) and laboratory mouse (I) embryos. Red boxes denote zoomed-in regions. (J-K) Representative GFP and H&E stained transverse sections showing the distribution of SFRP2 and hair follicles in control and transgenic mice (J) as well as differences in hair follicle number (K) (N = 4; *** P < 0.001). Scale bars: 200µm (zoomed out) and 25µm (zoomed in) in (F and H); 200µm (zoomed out) and 50µm (zoomed in) in (G and I); and 50µm in (J). NT = neural tube.

readily detectable in epidermal cells from lateral and ventral regions of the embryo but were absent from cells above the neural tube and adjacent areas, where *Sfrp2* expression was highest (**Fig. 3G**). This pattern contrasted with what was seen in stage-matched laboratory mouse embryos (E15.5), which had overall lower levels of dermal *Sfrp2* expression (**Fig. 3H**) and uniform levels of LEF1 and CTNNB1 throughout the epidermis, including above the neural tube (**Fig. 3I**). Taken together, our scRNA-seq data coupled to RNA *in situ*/IF analysis indicate that *Sfrp2* and Wnt signaling are negatively correlated and suggest that dermal *Sfrp2* expression acts to inhibit Wnt signaling in striped mouse embryonic skin.

Sfrp2 overexpression alters placode formation in laboratory mice

Wnt signaling is a primary determinant of hair follicle formation and spacing, as perturbation of members of this pathway leads to alterations in hair follicle number and distribution (*15*, *16*, *27*, *28*). This raises the intriguing hypothesis that *Sfrp2* may be acting to directly regulate striped mouse placode development. If this is the case, one would predict that increasing expression of *Sfrp2* in embryonic skin with low endogenous levels of *Sfrp2*, such as that of laboratory mouse (*25*, *26*), should alter placode formation. To test this, we generated $Rosa^{Sfrp2\text{-}GFP}$ mice, a strain that allowed us to activate *Sfrp2* transcription in the presence of a tissue-specific Cre drivers. To establish whether dermal expression of *Sfrp2* was sufficient to regulate placode formation, as implied by our striped mouse data, we crossed $Rosa^{Sfrp2\text{-}GFP}$ mice with *Dermo-Cre* mice, a mesenchymal driver of Cre (*29*, *30*) (**Fig. 3J**). Indeed, double-transgenic embryos (*Dermo-Cre*;$Rosa^{Sfrp2\text{-}GFP}$) analyzed at E17.5 showed a significant reduction in the number of placodes/hair follicles, compared to control littermates (N= 4) (**Fig. 3J, K**). Thus, our transgenic experiments in laboratory mice demonstrate a functional relationship between *Sfrp2* and embryonic placode development in which elevated levels of *Sfrp2* in the dermis leads to a marked reduction in the number of placodes/hair follicles.

The establishment of the *Sfrp2* dorsoventral gradient

In striped mice, *Sfrp2* is expressed in a dorsoventral gradient at E16.5, a stage coinciding with the emergence of embryonic placodes. To understand how such a pattern is established in space and time, we characterized the expression dynamics of *Sfrp2* by performing additional scRNA-seq analysis from the days prior to E16.5 (**Fig. 4A**). We found that the number of fibroblasts expressing *Sfrp2* was lowest at the earliest time-point sampled, E13.5 (36.03%), and gradually increased in subsequent days (40.03% at E14.5, 45.34% at E15.5, and 44.23% at E16.5) (Spearman correlation=0.79) (**Fig. 4B**). Moreover, average *Sfrp2* expression levels within those fibroblasts also increased during this period (**Fig. 4B**). In agreement with these observations, we observed a marked change in *Sfrp2* expression in a developmental trajectory of dermal fibroblasts modeled in latent time. Specifically, *Sfrp2* exhibited a prominent spatiotemporal increase across development toward R1-R3 regions at E16.5, having higher levels of expression in the region closest to the dorsal midline relative to the more lateral regions (*i.e.*, R1>R2 and R2>R3) (**Fig. 4C**).

We next asked whether the sharp increase in *Sfrp2* expression prior to placode formation was a unique feature of striped mice or, instead, a conserved process in rodent skin development. To address this, we performed scRNA-seq on laboratory mouse dorsal skin from multiple stages, including those preceding placode formation as well as at stages when placodes have formed (E12.5-E15.5) (**Fig. 4D**). In stark contrast to what was observed in striped mice, we found that the percentage of *Sfrp2*-expressing fibroblasts was highest early on (48.44% at E12.5) and decreased in subsequent days (28.44% at E15.5) (Spearman correlation=-0.78). In addition, average *Sfrp2* expression levels within fibroblasts also decreased from E13.5-E15.5 (**Fig. 4E**). Lastly, contrary

to what we found in striped mice, *Sfrp2* expression levels in laboratory mice fibroblasts showed no substantial change in latent time (**Fig. 4F**).

Together, our results indicate that *Sfrp2* levels in the dorsal mesenchyme of striped mice gradually increase prior to placodes becoming visible and reach peak numbers at the onset of placode formation. In line with our mathematical model and transgenic experiments, increased *Sfrp2* levels are sufficient to modulate the underlying developmental program controlling hair follicle formation. Moreover, our comparative analysis reveals opposing dynamics in laboratory mice, where *Sfrp2* expression levels decrease as placode formation nears, thereby allowing this process to proceed uniformly across the dorsal skin.

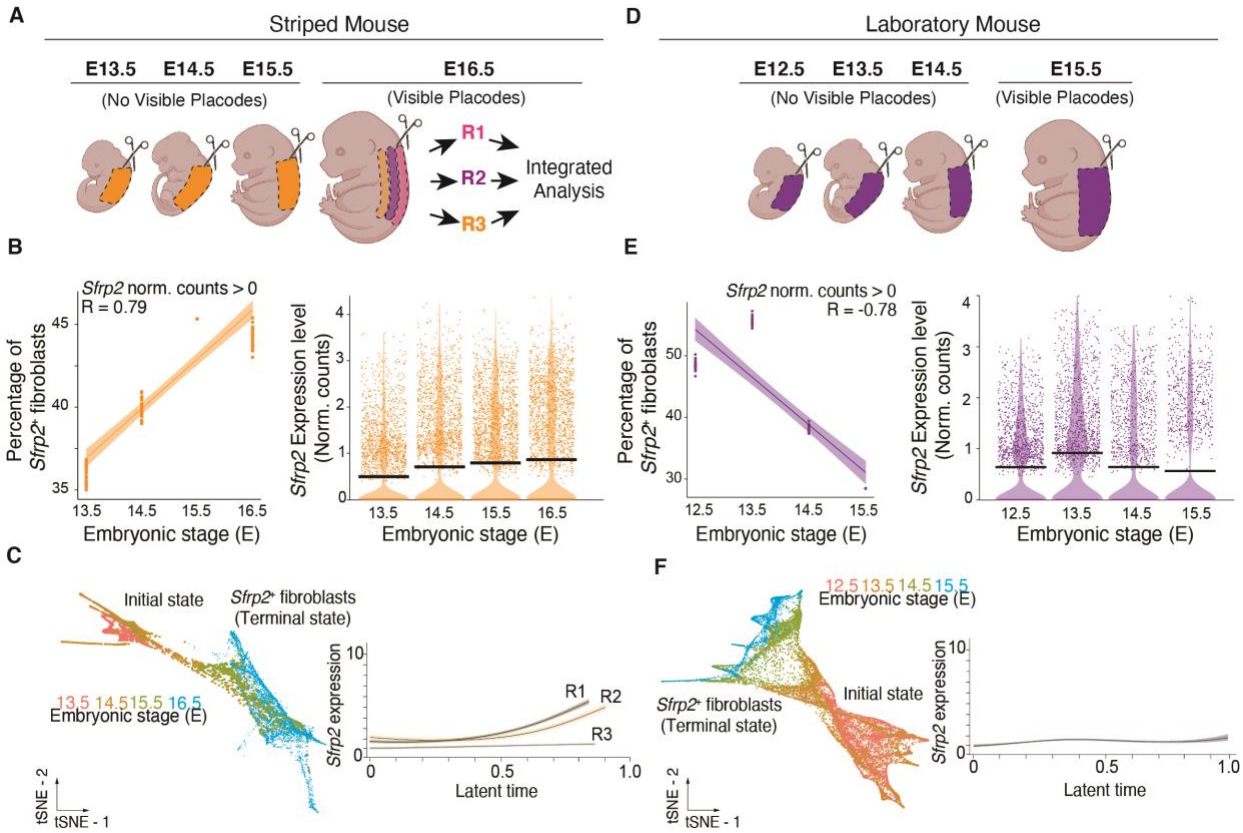

Fig. 4. Spatial and temporal *Sfrp2* expression patterns in striped mice and lab mice. (A) Schematic of striped mouse skin dissections from different developmental stages. For E16.5, scRNA-seq was performed on each individual region and data were pooled for an integrated analysis representative of whole striped mouse dorsal skin. (B) Both the percentage of fibroblasts that express *Sfrp2* (left, Spearman's Correlation, R = 0.79) and the expression levels of *Sfrp2* within those fibroblasts (right) increase in the days prior to visible placode formation in striped mouse dorsal skin. (C) Developmental trajectories inferred from striped mouse fibroblasts show regional differences in *Sfrp2* expression in latent time. (D) Schematic of laboratory mouse dissections from different developmental stages used for scRNA-seq. For all stages (E12.5-E15.5), whole dorsal skin was dissected (purple). (E) Both the percentage of fibroblasts expressing *Sfrp2* (left, Spearman's correlation, R = -0.78) and *Sfrp2* expression levels within those fibroblasts (right) decrease in the days prior to visible placode formation. (F) Developmental trajectories inferred from laboratory mouse fibroblasts show no substantial change in *Sfrp2* expression in latent time. Black lines in (B) and (E) indicate mean *Sfrp2* expression levels.

In vivo gene editing in striped mice leads to changes in coat pattern

If *Sfrp2* is indeed a key component of the dorsoventral gradient that organizes placode patterns, as our data suggest, changes in *Sfrp2* expression should alter such gradient and result in phenotypic changes to the stripe pattern. Indeed, changes in stripe width and number in response to decreasing modulator expression levels are a common feature of activator-inhibitor systems featuring modulated repression (**fig. S3**). In systems with narrow domains relative to pattern length scales, sensitivity to the gradient level is generally moderated by boundary conditions. Consequently, mathematical models with even order of magnitude changes in modulator concentration predict subtle alterations in stripe spacing (**Fig. 5A**).

To directly test the predictions from our model, we adapted a CRISPR-based experimental strategy in which recombinant adeno-associated viruses (rAAVs) are used to deliver CRISPR-CAS9 reagent into the oviduct of pregnant females. This *in vivo* gene editing technique is based on the ability of rAAVs to transduce the zona pellucida on intact pre-implantation embryos (*31*) (**Fig. 5B**). First, to establish the feasibility of using this approach for inducing gene knockouts in striped mice, we injected pregnant females carrying pre-implantation embryos with an rAAV packaged with Nme2Cas9 and a single-guide RNA (sgRNA) expression cassettes directed to the coding sequence of *Tyrosinase* (*Tyr*), the rate limiting enzyme for melanin production (*32*, *33*). Visual inspection of pups coupled to genotyping revealed this approach resulted in efficient gene editing, enabling us to generate complete knockout animals (**Fig. 5C**). To our knowledge, this is the first time that *in vivo* gene editing has been performed in a wild-derived mammalian species.

Encouraged by our proof-of-principle results, we next designed multiple sgRNA's against the 5' coding region of *Sfrp2* (**fig. S5A**). We then tested each sgRNA in striped mouse immortalized dermal fibroblasts and chose the one that had the highest indel-inducing efficiency. Next, we injected an rAAV containing Nme2Cas9 and sg*Sfrp2* expression cassettes into the oviducts of plugged females. From a total of 21 females injected, we obtained 57 pups, 14 of which carried gene edits in *Sfrp2*. After mating F0 founders and wildtype animals ($Sfrp2^{+/+}$) to ensure germline transmission, we crossed F1 heterozygous animals ($Sfrp2^{+/-}$) to generate F2 *Sfrp2* knockout ($Sfrp2^{-/-}$) mice. We used western blot to confirm the successful elimination of SFRP2 protein (**fig. S5B**). Analysis of coat phenotypes from early postnatal (P3) stages revealed significant and consistent differences in the coat patterns of F2 $Sfrp2^{-/-}$ and $Sfrp2^{+/+}$ striped mice. Specifically, we observed significant changes in the relative width of the stripes, with $Sfrp2^{-/-}$ mice having a narrower middle stripe and wider dark stripes than $Sfrp2^{+/+}$ mice, while light stripes remained unchanged (**Fig. 5D, E**). Notably, these phenotypes match remarkably well to our model predictions (**Fig 5A, D**). Thus, by knocking out *Sfrp2*, the dorsoventral organizing gradient is perturbed, effectively altering the boundaries of the striped mouse's coat pattern.

Sfrp2 regulates pigmentation via activation of Wnt signaling

In addition to changes in stripe pattern, we noticed that mutant animals had obvious differences in coat coloration, with $Sfrp2^{-/-}$ mice showing overall lighter pigmentation than $Sfrp2^{+/+}$ mice (**Fig. 5F, G**). Previous studies have shown that pigment production/melanogenesis can be controlled by Wnt signals secreted from the dermal papilla (*34*, *35*), a specialized mesenchymal component of the hair follicle that signals to pigment-producing cells, or melanocytes. Thus, to explore a potential link between *Sfrp2* and melanogenesis, we analyzed the skin of striped mice at P4, a period in which pigment is being actively synthesized and deposited in the growing hair shaft. Fluorescent *in situ* hybridizations on skin sections revealed that *Sfrp2* was specifically expressed in the dermal papilla (**fig. S6A**). Next, to test the effect of *Sfrp2* expression on

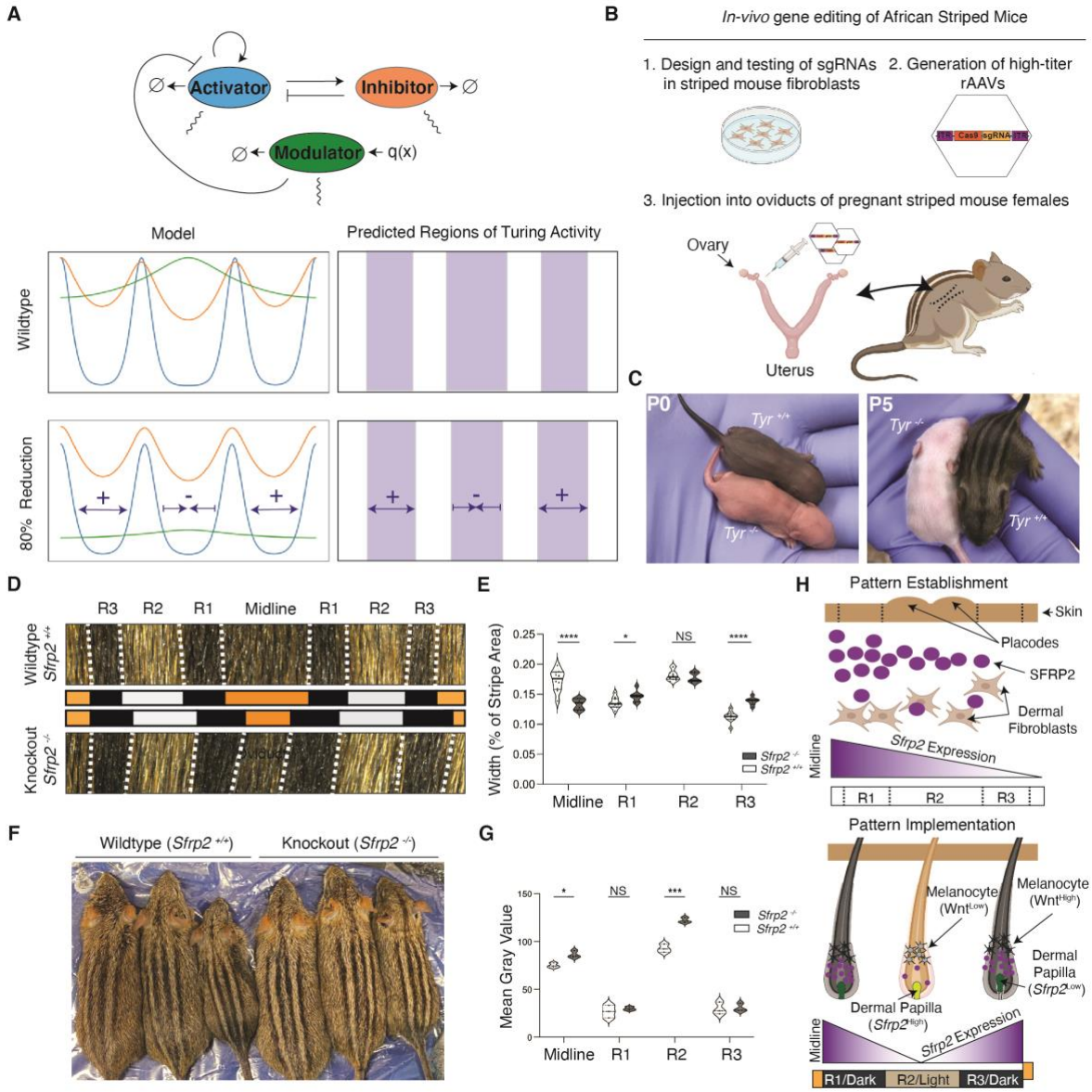

Fig. 5. *In vivo* genome editing reveals that *Sfrp2* regulates striped mouse coat patterns. (A) Simulations of reducing modulator concentration produce changes in the width of regions of Turing activity. Arrows indicate whether stripe width is predicted to increase (+) or decrease (-). (B) Schematic of the *in vivo* gene editing method used. (C) Postnatal Day 0 (P0) and P5 *Tyrosinase* wildtype ($Tyr^{+/+}$) and knockout ($Tyr^{-/-}$) striped mouse littermates. (D-E) *Sfrp2* regulates stripe pattern width. Shown are representative images (D) and measurements (E) revealing differences in stripe width between wildtype ($Sfrp2^{+/+}$) and *Sfrp2* knockout ($Sfrp2^{-/-}$) pups. Statistical significance in (E) (**** $P < 0.0001$; *** $P < 0.001$; ** $P < 0.01$; *$P < 0.05$; $Sfrp2^{+/+}$, N = 10; $Sfrp2^{-/-}$, N = 7) was assessed using an ANOVA test. (F) Representative differences in coat color between $Sfrp2^{+/+}$ and $Sfrp2^{-/-}$ adult mice taken as a single image. (F) Quantification of pigmentation between $Sfrp2^{+/+}$ and $Sfrp2^{-/-}$ adult mice reveal stripe-specific changes in color. Statistical significance in panel (F) (*** $P < 0.001$; *$P < 0.05$; $Sfrp2^{+/+}$, N = 3; $Sfrp2^{-/-}$, N = 3). (H) Model describing the role of *Sfrp2* in establishing (top) and implementing (bottom) the coat pattern in striped mice.

melanocytes, we stably transduced an immortalized mouse melanocyte cell line (Melan-A) with a lentiviral vector carrying the *Sfrp2* cDNA and used qPCR to measure the expression of *Tyr* and *Mitf*, two genes that promote melanin synthesis (*32*, *36*). Compared to melanocytes transduced with a control virus, cells overexpressing *Sfrp2* showed a significant increase in *Tyr* and *Mitf* (**fig. S6B**). Moreover, they also had marked increases in Wnt target genes, including *Axin2*, *C-myc*, and *Ccnd1* (*37–39*). Notably, these results are consistent with previous findings, in which recombinant SFRP2 was found to induce melanin synthesis in human primary melanocytes, via Wnt signaling activation, and to promote darkening of skin explants (*21*).

Since *Sfrp2* promotes melanin synthesis in postnatal stages, we next asked whether expression levels of this gene differed between striped regions (*i.e.*, stripes of different color). Using qPCR measurements from dissected P4 stripe skin regions, we found that *Sfrp2* was significantly lower in the light stripes (R2) compared to the flanking dark stripes (R1 and R3) (**fig. S6C**), an expression pattern drastically different from the dorsoventral gradient during mid-embryogenesis. Indeed, a time course analysis showed that *Sfrp2* expression in skin is temporally dynamic, shifting from a 'high-low' dorsoventral gradient at E16.5 to the 'high-low-high' pattern seen at P4 (**fig. S6C**). Taken together, our spatial expression data and *in vitro* functional experiments indicate that, during postnatal stages, *Sfrp2* undergoes a drastic shift in spatial expression and acts to promote melanogenesis via Wnt activation, thereby revealing an additional regulatory function during stripe pattern formation.

Discussion

In birds and mammals, periodic pigment patterns arise from two sequential processes: the first occurs early in embryogenesis and specifies the positional boundaries of the future pattern (*i.e., pattern establishment, or prepattern*); the second implements this prepattern through genes mediating pigment production during hair growth and cycling, giving rise to the observed color differences (*i.e., pattern implementation*) (*11*, *40*). Here, we identify *Sfrp2* as a regulator of both the establishment of the pre-pattern and its implementation, a dual role that is made possible by its dynamic expression pattern throughout embryogenesis and early postnatal stages and its opposing effects on Wnt signaling (**Fig. 5H**). The involvement of *Sfrp2* at multiple stages of pattern formation implies a fine-tuned spatiotemporal regulatory control, likely achieved through a complex *cis*-regulatory architecture and the action of multiple binding factors (*41*).

Secreted frizzled-related proteins (SFRPs) are known regulators of Wnt signaling that can exert their effects through a wide variety of mechanisms, including Wnt ligand sequestering, binding to Frizzled receptors, stabilization of Wnt-Frizzled complexes, and direct activation of Frizzled (*20*). As such, SFRPs can either inhibit or activate Wnt signaling, and their effect is dependent on cell type, developmental stage, and cellular microenvironment (*20*). In striped mice, embryonic expression of *Sfrp2* in a subset of dermal fibroblasts causes a decrease of epidermal CTNNB1 and LEF1, leading to alterations in placode number (**Fig. 5H**). Later in development, dermal papilla-specific expression of *Sfrp2* alters melanocyte behavior, causing an increase in the expression of Wnt targets and genes involved in melanogenesis (**Fig. 5H**). Thus, our results show that *Sfrp2* can lead to opposing regulation (i.e., activation and inhibition) of Wnt signaling within the same tissue.

It is noteworthy that elimination of *Sfrp2* led to a subtle, albeit consistent difference in the coat pattern of striped mice. This result is not surprising, as subtle changes in stripe width are consistent with predictions from our simulations. Moreover, it is likely that there are additional reinforcing/redundant mechanisms at play that act in concert to establish the dorsoventral orienting

gradient and assure phenotypic robustness. For example, our bulk-level RNA-seq data from E16.5 embryos shows that there are additional Wnt inhibitors which are also expressed in a dorsoventral gradient, such as *Dkk2*, *Igfb4*, *Rspo2*, and *Rspo4* (**fig. S4**). Such molecules may act in coordination with *Sfrp2* to specify patterns of placode morphogenesis and are therefore still playing a substantial role in regulating this trait in *Sfrp2*$^{-/-}$ striped mice. Similarly, with respect to pigmentation, our previous work showed that hair color differences in striped mice are controlled by the interplay of melanocyte-autonomous (e.g., *Alx3*-mediated suppression of melanocyte differentiation) and non-autonomous processes (e.g., regulation of pigment-type switching by paracrine factors secreted from the dermal papilla, including *Asip* and *Edn3*) (*10*, *35*). Thus, although *Sfrp2* influences pigmentation, as our experiments show, it is clear that modulation of hair color in striped mice is achieved through the combinatorial effect of multiple genes (*10*).

By integrating multidisciplinary approaches, our work reveals insights into the mechanisms by which spatial patterns are established in developing embryos. In addition, by extending *in vivo* genome editing approaches to wild-derived striped mice, a technique previously restricted to traditional mammalian laboratory models (*i.e.*, laboratory mouse and rats), our work exemplifies the potential of using emerging model species to uncover the mechanistic basis of naturally evolved phenotypic traits and will open the door for functional studies in other mammals.

References

1. T. Caro, The Adaptive Significance of Coloration in Mammals. *Bioscience*. **55**, 125–136 (2005).
2. M. G. Mills, L. B. Patterson, Not just black and white: pigment pattern development and evolution in vertebrates. *Semin. Cell Dev. Biol.* **20**, 72–81 (2009).
3. T. Caro, R. Mallarino, Coloration in Mammals. *Trends Ecol. Evol.* **35**, 357–366 (2020).
4. S. Kondo, T. Miura, Reaction-Diffusion Model as a Framework for Understanding Biological Pattern Formation. *Science*. **329**, 1616–1620 (2010).
5. S. Kondo, An updated kernel-based Turing model for studying the mechanisms of biological pattern formation. *J. Theor. Biol.* **414**, 120–127 (2017).
6. A. M. Turing, The chemical basis of morphogenesis. 1953. *Bull. Math. Biol.* **52**, 153–97; discussion 119-52 (1990).
7. S. T. Vittadello, T. Leyshon, D. Schnoerr, M. P. H. Stumpf, Turing pattern design principles and their robustness. *Philosophical Transactions of the Royal Society A: Mathematical, Physical and Engineering Sciences*. **379**, 20200272 (2021).
8. L. B. Patterson, D. M. Parichy, Zebrafish Pigment Pattern Formation: Insights into the Development and Evolution of Adult Form. *Annu. Rev. Genet.* **53**, 505–530 (2019).
9. C. B. Kaelin, K. A. McGowan, G. S. Barsh, Developmental genetics of color pattern establishment in cats. *Nat. Commun.* **12**, 5127 (2021).
10. R. Mallarino, C. Henegar, M. Mirasierra, M. Manceau, C. Schradin, M. Vallejo, S. Beronja, G. S. Barsh, H. E. Hoekstra, Developmental mechanisms of stripe patterns in rodents. *Nature*. **539**, 518–523 (2016).
11. N. Haupaix, M. Manceau, The embryonic origin of periodic color patterns. *Dev. Biol.* **460**, 70–76 (2020).
12. C. B. Kaelin, X. Xu, L. Z. Hong, V. A. David, K. A. McGowan, A. Schmidt-Küntzel, M. E. Roelke, J. Pino, J. Pontius, G. M. Cooper, H. Manuel, W. F. Swanson, L. Marker, C. K. Harper, A. van Dyk, B. Yue, J. C. Mullikin, W. C. Warren, E. Eizirik, L. Kos, S. J. O'Brien,

G. S. Barsh, M. Menotti-Raymond, Specifying and sustaining pigmentation patterns in domestic and wild cats. *Science*. **337**, 1536–1541 (2012).
13. R. Mallarino, N. Pillay, H. E. Hoekstra, C. Schradin, African striped mice. *Curr. Biol.* **28**, R299–R301 (2018).
14. M. H. Hardy, The secret life of the hair follicle. *Trends Genet.* **8**, 55–61 (1992).
15. S. E. Millar, Molecular mechanisms regulating hair follicle development. *J. Invest. Dermatol.* **118**, 216–225 (2002).
16. T. Andl, S. T. Reddy, T. Gaddapara, S. E. Millar, WNT signals are required for the initiation of hair follicle development. *Dev. Cell*. **2**, 643–653 (2002).
17. T. W. Hiscock, S. G. Megason, Orientation of Turing-like Patterns by Morphogen Gradients and Tissue Anisotropies. *Cell Syst.* **1**, 408–416 (2015).
18. S. Sick, S. Reinker, J. Timmer, T. Schlake, WNT and DKK determine hair follicle spacing through a reaction-diffusion mechanism. *Science*. **314**, 1447–1450 (2006).
19. R. A. Van Gorder, Pattern formation from spatially heterogeneous reaction-diffusion systems. *Philos. Trans. A Math. Phys. Eng. Sci.* **379**, 20210001 (2021).
20. K. van Loon, E. J. M. Huijbers, A. W. Griffioen, Secreted frizzled-related protein 2: a key player in noncanonical Wnt signaling and tumor angiogenesis. *Cancer Metastasis Rev.* **40**, 191–203 (2021).
21. M. Kim, J. H. Han, J.-H. Kim, T. J. Park, H. Y. Kang, Secreted Frizzled-Related Protein 2 (sFRP2) Functions as a Melanogenic Stimulator; the Role of sFRP2 in UV-Induced Hyperpigmentary Disorders. *J. Invest. Dermatol.* **136**, 236–244 (2016).
22. C.-J. Liang, Z.-W. Wang, Y.-W. Chang, K.-C. Lee, W.-H. Lin, J.-L. Lee, SFRPs Are Biphasic Modulators of Wnt-Signaling-Elicited Cancer Stem Cell Properties beyond Extracellular Control. *Cell Rep.* **28**, 1511-1525.e5 (2019).
23. H. Lin, M. Angeli, K. J. Chung, C. Ejimadu, A. R. Rosa, T. Lee, sFRP2 activates Wnt/β-catenin signaling in cardiac fibroblasts: differential roles in cell growth, energy metabolism, and extracellular matrix remodeling. *Am. J. Physiol. Cell Physiol.* **311**, C710–C719 (2016).
24. K. Gupta, J. Levinsohn, G. Linderman, D. Chen, T. Y. Sun, D. Dong, M. M. Taketo, M. Bosenberg, Y. Kluger, K. Choate, P. Myung, Single-Cell Analysis Reveals a Hair Follicle Dermal Niche Molecular Differentiation Trajectory that Begins Prior to Morphogenesis. *Dev. Cell*. **48**, 17-31.e6 (2019).
25. R. Sennett, Z. Wang, A. Rezza, L. Grisanti, N. Roitershtein, C. Sicchio, K. W. Mok, N. J. Heitman, C. Clavel, A. Ma'ayan, M. Rendl, An Integrated Transcriptome Atlas of Embryonic Hair Follicle Progenitors, Their Niche, and the Developing Skin. *Dev. Cell*. **34**, 577–591 (2015).
26. A. Rezza, Z. Wang, R. Sennett, W. Qiao, D. Wang, N. Heitman, K. W. Mok, C. Clavel, R. Yi, P. Zandstra, A. Ma'ayan, M. Rendl, Signaling Networks among Stem Cell Precursors, Transit-Amplifying Progenitors, and their Niche in Developing Hair Follicles. *Cell Rep.* **14**, 3001–3018 (2016).
27. S.-Y. Tsai, R. Sennett, A. Rezza, C. Clavel, L. Grisanti, R. Zemla, S. Najam, M. Rendl, Wnt/β-catenin signaling in dermal condensates is required for hair follicle formation. *Dev. Biol.* **385**, 179–188 (2014).
28. U. Gat, R. DasGupta, L. Degenstein, E. Fuchs, De Novo hair follicle morphogenesis and hair tumors in mice expressing a truncated beta-catenin in skin. *Cell*. **95**, 605–614 (1998).
29. K. Yu, J. Xu, Z. Liu, D. Sosic, J. Shao, E. N. Olson, D. A. Towler, D. M. Ornitz, Conditional inactivation of FGF receptor 2 reveals an essential role for FGF signaling in the regulation of osteoblast function and bone growth. *Development*. **130**, 3063–3074 (2003).

30. D. Šošić, J. A. Richardson, K. Yu, D. M. Ornitz, E. N. Olson, Twist Regulates Cytokine Gene Expression through a Negative Feedback Loop that Represses NF-κB Activity. *Cell*. **112**, 169–180 (2003).
31. Y. Yoon, D. Wang, P. W. L. Tai, J. Riley, G. Gao, J. A. Rivera-Pérez, Streamlined ex vivo and in vivo genome editing in mouse embryos using recombinant adeno-associated viruses. *Nat. Commun.* **9**, 1–12 (2018).
32. K. Iozumi, G. E. Hoganson, R. Pennella, M. A. Everett, B. B. Fuller, Role of tyrosinase as the determinant of pigmentation in cultured human melanocytes. *J. Invest. Dermatol.* **100**, 806–811 (1993).
33. A. Edraki, A. Mir, R. Ibraheim, I. Gainetdinov, Y. Yoon, C.-Q. Song, Y. Cao, J. Gallant, W. Xue, J. A. Rivera-Pérez, E. J. Sontheimer, A Compact, High-Accuracy Cas9 with a Dinucleotide PAM for In Vivo Genome Editing. *Mol. Cell*. **73**, 714-726.e4 (2019).
34. D. Enshell-Seijffers, C. Lindon, E. Wu, M. M. Taketo, B. A. Morgan, β-Catenin activity in the dermal papilla of the hair follicle regulates pigment-type switching. *Proceedings of the National Academy of Sciences*. **107**, 21564–21569 (2010).
35. B. A. Morgan, The dermal papilla: an instructive niche for epithelial stem and progenitor cells in development and regeneration of the hair follicle. *Cold Spring Harb. Perspect. Med.* **4**, a015180 (2014).
36. E. Steingrímsson, N. G. Copeland, N. A. Jenkins, Melanocytes and the microphthalmia transcription factor network. *Annu. Rev. Genet.* **38**, 365–411 (2004).
37. E.-H. Jho, T. Zhang, C. Domon, C.-K. Joo, J.-N. Freund, F. Costantini, Wnt/beta-catenin/Tcf signaling induces the transcription of Axin2, a negative regulator of the signaling pathway. *Mol. Cell. Biol.* **22**, 1172–1183 (2002).
38. M. Shtutman, J. Zhurinsky, I. Simcha, C. Albanese, M. D'Amico, R. Pestell, A. Ben-Ze'ev, The cyclin D1 gene is a target of the beta-catenin/LEF-1 pathway. *Proc. Natl. Acad. Sci. U. S. A.* **96**, 5522–5527 (1999).
39. T. C. He, A. B. Sparks, C. Rago, H. Hermeking, L. Zawel, L. T. da Costa, P. J. Morin, B. Vogelstein, K. W. Kinzler, Identification of c-MYC as a target of the APC pathway. *Science*. **281** (1998), pp. 1509–1512.
40. C. B. Kaelin, G. S. Barsh, Genetics of pigmentation in dogs and cats. *Annu Rev Anim Biosci*. **1**, 125–156 (2013).
41. S. H. Keller, S. G. Jena, Y. Yamazaki, B. Lim, Regulation of spatiotemporal limits of developmental gene expression via enhancer grammar. *Proceedings of the National Academy of Sciences*. **117**, 15096–15103 (2020).
42. M. H. Kaufman, *The Atlas of Mouse Development* (Academic Press Limited, London, England, 1992).
43. J. Wu, X. Wang, Whole-Mount In Situ Hybridization of Mouse Embryos Using DIG-Labeled RNA Probes. *Methods Mol. Biol.* **1922**, 151–159 (2019).
44. Michael I Love, Wolfgang Huber, Simon Anders, Moderated estimation of fold change and dispersion for RNA-seq data with DESeq2. *Genome Biology* (2014).
45. J. R. Conway, A. Lex, N. Gehlenborg, UpSetR: an R package for the visualization of intersecting sets and their properties. *Bioinformatics*. **33**, 2938–2940 (2017).
46. A. Gierer, H. Meinhardt, A theory of biological pattern formation. *Kybernetik*. **12**, 30–39 (1972).
47. K. J. Burns, G. M. Vasil, J. S. Oishi, D. Lecoanet, B. P. Brown, Dedalus: A flexible framework for numerical simulations with spectral methods. *Phys. Rev. Res.* **2**, 023068 (2020).

48. C. Y. Feigin, A. H. Newton, L. Doronina, J. Schmitz, C. A. Hipsley, K. J. Mitchell, G. Gower, B. Llamas, J. Soubrier, T. N. Heider, B. R. Menzies, A. Cooper, R. J. O'Neill, A. J. Pask, Genome of the Tasmanian tiger provides insights into the evolution and demography of an extinct marsupial carnivore. *Nature Ecology & Evolution*. **2**, 182–192 (2017).
49. H. Li, A statistical framework for SNP calling, mutation discovery, association mapping and population genetical parameter estimation from sequencing data. *Bioinformatics*. **27**, 2987–2993 (2011).
50. S. L. Wolock, R. Lopez, A. M. Klein, Scrublet: Computational Identification of Cell Doublets in Single-Cell Transcriptomic Data. *Cell Syst*. **8**, 281-291.e9 (2019).
51. J. Fan, N. Salathia, R. Liu, G. E. Kaeser, Y. C. Yung, J. L. Herman, F. Kaper, J.-B. Fan, K. Zhang, J. Chun, P. V. Kharchenko, Characterizing transcriptional heterogeneity through pathway and gene set overdispersion analysis. *Nat. Methods*. **13**, 241–244 (2016).
52. T. Stuart, A. Butler, P. Hoffman, C. Hafemeister, E. Papalexi, W. M. Mauck 3rd, Y. Hao, M. Stoeckius, P. Smibert, R. Satija, Comprehensive Integration of Single-Cell Data. *Cell*. **177**, 1888-1902.e21 (2019).
53. M. Lange, V. Bergen, M. Klein, M. Setty, B. Reuter, M. Bakhti, H. Lickert, M. Ansari, J. Schniering, H. B. Schiller, D. Pe'er, F. J. Theis, CellRank for directed single-cell fate mapping. *Nat. Methods*. **19**, 159–170 (2022).
54. S. Beronja, G. Livshits, S. Williams, E. Fuchs, Rapid functional dissection of genetic networks via tissue-specific transduction and RNAi in mouse embryos. *Nat. Med.* **16**, 821–827 (2010).
55. T. Aasen, J. C. Izpisúa Belmonte, Isolation and cultivation of human keratinocytes from skin or plucked hair for the generation of induced pluripotent stem cells. *Nat. Protoc.* **5**, 371–382 (2010).
56. W. C. Hahn, S. K. Dessain, M. W. Brooks, J. E. King, B. Elenbaas, D. M. Sabatini, J. A. DeCaprio, R. A. Weinberg, Enumeration of the simian virus 40 early region elements necessary for human cell transformation. *Mol. Cell. Biol.* **22**, 2111–2123 (2002).
57. J.-P. Concordet, M. Haeussler, CRISPOR: intuitive guide selection for CRISPR/Cas9 genome editing experiments and screens. *Nucleic Acids Res.* **46**, W242–W245 (2018).
58. M. Sato, Intraoviductal introduction of plasmid DNA and subsequent electroporation for efficient in vivo gene transfer to murine oviductal epithelium. *Mol. Reprod. Dev.* **71**, 321–330 (2005).

Acknowledgments
We thank members of the Mallarino lab; Princeton LAR (Chris Dmytrow, Kirsten Gerhart, Grace Barnett, and Jamus McGuire) for help with striped mice husbandry; the LSI Genomics Core (Wei Wang, Jennifer M. Miller, Jessica Wiggins, and Jean Arley Volmar) for help with library preparation and sequencing; the Nikon Center of Excellence Confocal Microscopy Core (Gary Laevsky, Sha Wang); and members of the Rivera-Perez lab (Yeonsoo Yoon and Judith Gallant) for help with *in vivo* genome editing experiments. We also thank Eric F. Wieschaus, Girish Deshpande, and Philipp Holl for insights and discussion.

Funding
This project was supported by an NIH grant to RM (R35GM133758). MRJ was supported by an NIH fellowship (F32 GM139253). SL was supported by a Presidential Postdoctoral Research fellowship (Princeton University). BB was supported by an NIH training grant (T32GM007388). CF was supported by an NIH fellowship (F32 GM139240-01). C.F.G-J. is partially supported by

UC Irvine Chancellor's ADVANCE Postdoctoral Fellowship Program. QN was partially supported by an NSF grant DMS1763272 and a Simons Foundation grant (594598).

Author contributions

MRJ and RM conceived the project and designed experiments. MRJ performed all RNA sequencing experiments and bulk RNA sequencing analysis. SL performed the *in vitro* and *in vivo* genome editing in striped mice, with help from SAM and JAR-P. MRJ and SL performed all downstream processing and analysis of genome edited animals. PM and SYS did the mathematical modeling. CFG-J led the scRNAseq analysis, with support from MRJ and QN. MRJ and RM performed *in situ* hybridizations. MRJ, SAM, and BB performed the phenotypic characterization of striped mouse and laboratory mouse tissues, including immunofluorescence and histology. MRJ and SAM performed the melanocyte cell culture experiments. CF generated the "*Rhabdomyzed" Mus* genome and Liftover annotation. JG and AP generated the immortalized *Rhabdomys* fibroblasts. MRJ and RM wrote the manuscript with input from all authors.